Suprasalt model building using full-waveform inversion

Dhananjay Tiwari[1], Jian Mao[1], and James Sheng[1]

https://doi.org/10.1190/tle38030214.1.

Abstract

The application of full-waveform inversion (FWI) to bring high resolution to the velocity model is becoming a standard approach in the velocity model-building workflow. Diving wave FWI in conjunction with reflection FWI (RFWI) has been widely used in the Gulf of Mexico (GOM) to optimize the suprasalt model. Accuracy of a velocity model from tomography is dependent on residual moveout (RMO) picking accuracy. In a good signal-to-noise ratio area, the confidence of RMO picking is high. But gathers in areas affected by gas exhibit poor event continuity, which makes it difficult to get accurate RMO picks. In such a geologic regime, FWI can improve the velocity model and therefore the final image quality. There are two main components of a velocity model from the GOM area: the first is the sediment, and the second is salt geometry. In the beginning of the model-building cycle, it is most likely that salt geometry is not accurately defined. This inaccuracy leads to a big mismatch between synthetic and observed data for both diving wave FWI and RFWI. One way to handle this situation is to start with the salt model and iteratively adjust the salt interpretation as FWI model building progresses from lower to higher frequencies. Another approach could be eliminating the salt-related energy from the input and then using the sediment-only model for FWI. We are proposing a desalt approach in which we try to eliminate or reduce the salt-related energy from the input data and then use a sediment-only velocity model as a starting model for the entire suprasalt FWI workflow. We will present a case study in which, by adapting the desalt workflow, we could manage to do more FWI iterations by eliminating salt interpretation.

Introduction

Wide-azimuth (WAZ) data in the Gulf of Mexico (GOM) area have proven to be advantageous over conventional narrow-azimuth data in terms of better subsurface illumination and fold coverage.

Deriving a velocity model using the tomography approach is still the most cost-effective and widely acceptable approach across the industry. Over the past couple of years, the industry has derived and adopted an advanced model-building and imaging approach to improve the overall velocity model and final seismic image. For example, when in the presence of orthogonal WAZ surveys, extending model building from vertical transverse isotropy/tilted transverse isotropy (TTI) to orthorhombic to resolve the azimuthal variation of seismic velocity properties associated with slow and fast velocity direction is a wise choice to realize the best results from expensive orthogonal WAZ acquisition.

Reliability of derived models using tomography depends on the accuracy of residual moveout (RMO) picked on the common-image gather (CIG), and therefore these methods tend to suffer in areas with poor signal-to-noise ratio (S/N). Tomography cannot bring high resolution to the velocity model even when S/N is good for RMO picking. Gas-charged sediment and shallow channels are a few geologic scenarios in which the model can be improved by using full-waveform inversion (FWI). We often see seismic-obscured areas in the GOM with little to no signal. These seismic-obscured areas, especially in the shallow zone, hamper deeper imaging due to unresolved velocity anomalies during the tomography workflow. Extending a model-building approach from conventional tomography to FWI can help bring the low-velocity anomaly associated with the gas-charged sediment into the velocity model as well as update the seismic-obscured areas we often see in the GOM. FWI works to minimize the differences between observed and synthetic data in terms of amplitude and phase (Lailly, 1983; Tarantola, 1984) by updating the velocity model. If the observed and synthetic differences are within the half cycle of wavelet, then FWI can still provide a desired update to the model without cycle skipping. It is in the best interest of diving wave FWI (DFWI) and reflection FWI (RFWI) to begin with a good background velocity model to mitigate cycle skipping in the beginning. A lack of signal at low frequency limits the FWI capabilities to derive long-wavelength updates for the velocity model. Tomography does an excellent job of updating the long-wavelength corrections to the velocity model. It is also able to derive the long-wavelength background velocity, compensating for the limitations of FWI due to the lack of low frequency in the input.

Interaction of reflection and refraction energy from the salt boundary with the suprasalt sediment creates a big mismatch between observed and synthetic data if the starting model is sediment. Possibilities of cycle skipping for FWI updates increase as the mismatch goes more toward a half wavelength between observed and synthetic seismic data. A salt model can be used as a starting model to minimize this effect to some extent. We can use the salt model as a starting model for FWI, and then an iterative approach of updating the salt model at every FWI update (Wang et al., 2015) can be used. But this approach is expensive when used for medium to large 3D seismic projects, especially if the target is to optimize the suprasalt velocity model. Another approach to handle the mismatch near the salt is to remove or attenuate the salt-related energy from the input data. Attenuating the energy associated with the salt boundary from the acquired seismic at the beginning of the project can help reduce the mismatch between observed and synthetic data while using the sediment model. Using this approach can save several iterations of adjusting the salt interpretation during FWI iterations and thus the overall cost. We have demonstrated a robust multistage FWI for high-resolution model building (Mao et al., 2016). Each shot in the WAZ data covers more area; therefore, a coarse-grid shot

[1]TGS, Houston, Texas, USA. E-mail: dhananjay.tiwari@tgs.com; jian.mao@tgs.com; james.sheng@tgs.com.

density can be used during the FWI workflow to optimize the cost and quality. We present an FWI case study using 3D WAZ data from the GOM, aiming to derive an improved velocity model by incorporating desalt to optimize overall FWI workflow in terms of cost and quality.

Survey area and data challenges

FWI is applied to more than 100 Outer Continental Shelf blocks in the Mississippi Canyon (Figure 1). One motivation to move forward with the FWI approach can be clearly understood from the data example shown in Figure 2. Figure 2a is a depth slice of seismic corendered with the underlying velocity model prior to FWI. The yellow highlighted area shows the low-velocity anomaly in the velocity model. Figures 2b and 2c show the cross-section view along the inline and crossline within the same survey. Clearly, both the inline and crossline show the underlying imaging challenges associated with the unresolved velocity anomaly highlighted in the circled area. There is hardly any visible reflected energy within the circled area on stack image migrated with the pre-FWI velocity model. Deriving the necessary velocity updates from the conventional tomography around the circled area is severely constrained by the poor S/N of the data, which makes it very difficult to get decent-quality RMO picks on CIGs for the tomography. Imaging is especially challenging in this area due to unresolved velocity modeling in several isolated zones with little to no reflection energy (reflections quiet zone) as shown in Figures 2b and 2c. In such a geologic environment, FWI can benefit in updating the model in a reflection quiet zone as FWI depends on the residual of recorded and synthetic seismic data rather than RMO picks. We anticipate that adding the FWI workflow will help resolve the underlying velocity model associated within the reflection quiet zone. Final imaging using the FWI updated velocity model will be enhanced within the seismic quiet zone as well as in the deeper section beneath these zones.

FWI model updates

Updating a model from FWI is a multistep process that can be broadly described in three steps for simplicity:

1) Derive a good initial velocity model for FWI by a conventional approach of model updating through a few iterations of tomography.
2) Input data preconditioning for FWI, which includes wavelet estimation and removal of the salt-related energy from the input.
3) Optimize the velocity model from FWI that may include a multistep process.
   a) Step 1. Dynamic warping (Ma and Hale, 2013) preconditioned FWI (DWFWI) works by preconditioning the observed data through dynamic warping to minimize the major traveltime residuals. DWFWI provides large-scale background velocity updates to mitigate cycle skipping between observed and synthetic seismic data.
   b) Step 2. Image-guided diving wave FWI (IGDFWI) uses image-guided smoothing to reduce the acquisition footprint and swing noise. It provides the high-resolution feature by utilizing the L2-norm objective function

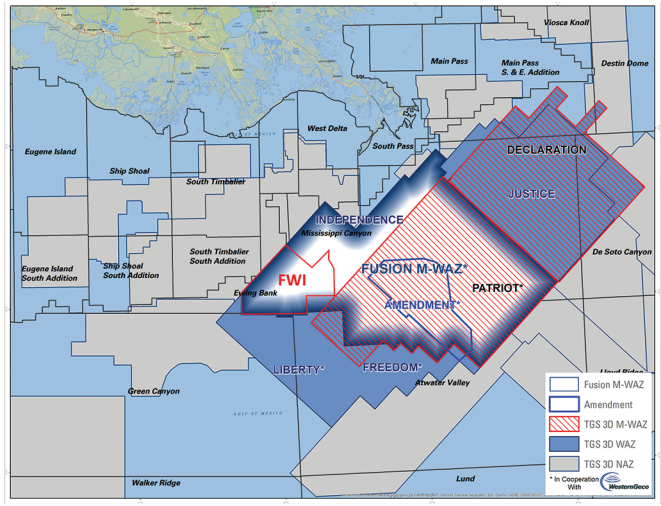

Figure 1. Survey area (fusion).

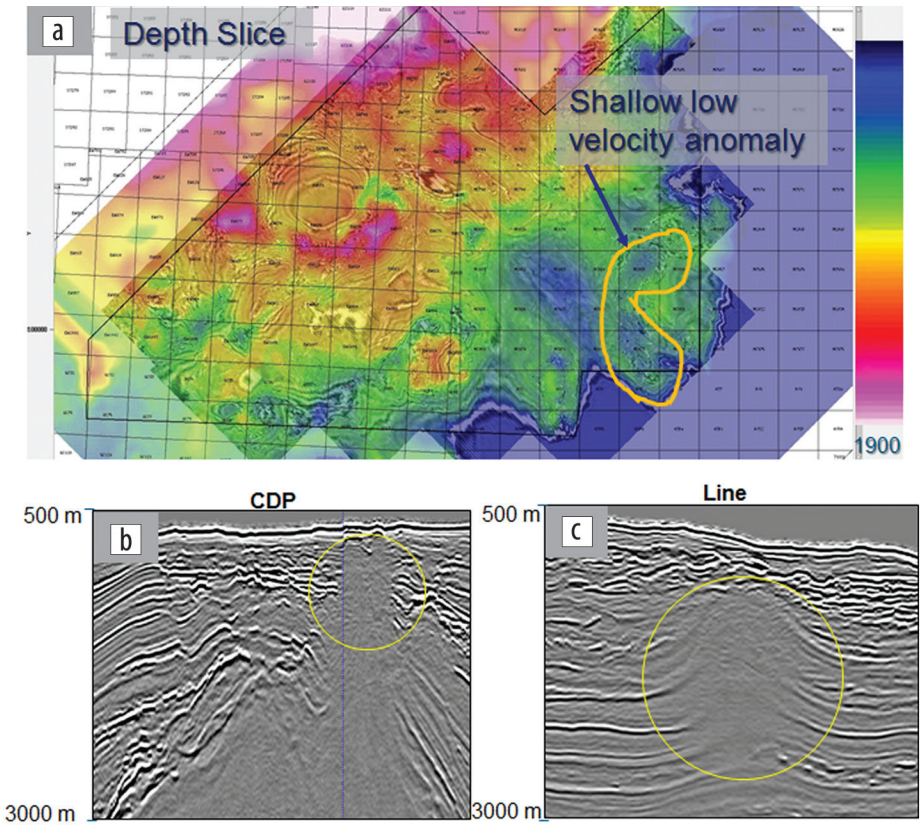

Figure 2. (a) Depth slice corendered with the underlying velocity model showing the low-velocity anomaly within the survey highlighted in yellow. (b) Inline and (c) crossline view of the KDM stack.

during FWI. A combination of DWFWI and IGDFWI provides more robust and high-resolution model updates for the shallow depth.

c) Step 3. Wavepath reflection FWI (WPRFWI) updates the velocity through reflection wavepaths. WPRFWI provides model updates to the deeper section.

d) Step 4. High-resolution reflection FWI (HRFWI) provides high-resolution features and sharp boundaries. Combining WPRFWI and HRFWI helps update high-resolution model updates for deeper depths (e.g., subsalt and complex salt overhang areas).

The four steps can be used for model updates from shallow to deep including the salt velocity updates. This paper particularly deals with suprasalt model building by using desalt inputs and sediment-only models for FWI.

Initial velocity model for FWI

A legacy anisotropic final velocity model smoothed and calibrated with the available check shot within the survey is used to run the prestack Kirchhoff depth migration (KDM) and first iteration of tomography. KDM gathers using an updated model from the first pass of tomography are then used in focusing analysis (Cai et al., 2009; He et al., 2009) to derive the anisotropic parameters.

The multi-WAZ data are then sectored into six azimuths to begin the azimuth-sectored tomography. We perform two passes of TTI tomography to optimize the suprasalt velocity model. The tomography-updated model is used as a starting model for FWI. We aim to bring the long-wavelength background velocity model updates to the starting model using the conventional approach of a tomography workflow. The aim of tomography-based model updates is to offset the unavailability of low frequency in the seismic data, which could have been used for FWI to resolve the overall background model instead of tomography. Tomography is a powerful tool that is widely used within the industry to optimize depth interval velocity models for depth imaging. But tomography alone cannot bring high-frequency details to the model and suffers when updating velocity models in which RMO pick confidence is low, for example in a poor S/N area. In our experience, tomography plus FWI can be considered as the best possible package to optimize the velocity model in geologically complex environments.

Input data preparation

Wavelet estimation is the first crucial part of the FWI workflow. A multistep process is used to derive the optimal wavelet for FWI. The initial wavelet is first optimized for a single line then for a small area before analyzing for whole surveys. Synthetic data are created for a line using the initial velocity model and initial wavelet. A matching filter operator is derived iteratively starting first for a line followed by a coarse-grid whole survey to optimize the wavelet that best matches synthetic and observed data.

DFWI relies on the diving wave energy recorded at the far offsets. During production, we normally try to isolate diving wave energy by muting reflection-related energy from the input shot. In the GOM area, these diving waves are often mixed with energy reflected from the salt boundary. If the salt bodies are deep, then the muting will still work well to keep the majority of diving wave energy during the DFWI. Isolating the salt-related energy becomes more challenging when the salt is relatively shallow as diving wave and seismic reflection from the salt are mixed together. This limits the use of DFWI when the objective is to update the suprasalt velocity model.

Interaction of reflection energy from the salt creates a significant mismatch between the observed and synthetic data, which will cause cycle skipping, and the FWI may end up converging to a local minimum instead of a global minimum. The large residuals caused by the salt-related energy can be minimized in two ways: a model-based approach and a data-domain approach by desalt.

Model based. During DFWI, the first focus is to update the shallow section of the sediment model before optimizing salt geometry and the complex salt overhang area. The presence of salt bodies often creates strong energy that interferes with the diving wave (Jones, 2014), which creates a big mismatch between observed and synthetic data.

To minimize the big mismatch between observed and synthetic data in the presence of salt, we may consider starting FWI by using the salt velocity model and iteratively adjusting the salt interpretation as we improve the model updates from FWI.

Data-domain approach by desalt. Another method is to remove or attenuate the salt-related energy from the input data and use a sediment-only model for suprasalt FWI model updates. Starting with the salt model and continually adjusting the salt model involves significant salt interpretation after every iteration of FWI updates. For a large to midsize project, the cost of the FWI model increases multifold using the model-based approach. We have adopted the second approach by attenuating the salt-related energy from the input in the beginning and using those data for all FWI iterations. We use the salt horizons from our library to build the salt model that is used to create the synthetic. We also create a synthetic from the sediment model. Synthetic data from the salt and sediment model were subtracted to get only reflection associated with the salt. The salt reflection is then adaptively subtracted from the input data after dynamic warping to attenuate the salt-related energy from the input data. We use adaptive subtraction to take care of kinematic inaccuracy of the salt-related energy between observed and synthetic seismic data caused by the incomplete salt geometry at the beginning of the project. Figure 3 shows the desalt workflow. There could be minor differences for the entire desalt workflow from one project to another depending on the accuracy of the initial salt geometry. Figure 4 shows an example of desalt. Figure 4a is the synthetic model from the salt model, and Figure 4b is the synthetic model from the sediment-only velocity model. A direct subtraction of these two synthetics will give the energy associated with the salt boundary (Figure 4c). The salt synthetic, as shown in Figure 4c, is adaptively subtracted from the input data (Figure 4d). Figure 4e is the output after the adaptive subtraction from the salt synthetic. The salt-related energy circled in Figure 4d is attenuated after the adaptive subtraction as shown in Figure 4e. To make the desalt cost effective, the highest frequency of the two synthetic models is kept close to FWI highest possible frequency. This way, we only need to create

the desalt input once, and then it can be used for all FWI iterations starting from low frequency to high frequency. Adaptive subtraction can be optimized further if we have a predetermined frequency band for FWI iterations. We can split input and synthetic into the frequency band that matches the FWI frequency band for the subtraction and then sum them together after the subtraction as we normally do during surface-related multiple elimination. The impact of desalt on the FWI model update near the salt boundary can be seen by comparing Figures 4f and 4g. Clearly the large model update (ΔV) near the salt is attenuated using the desalt input for FWI.

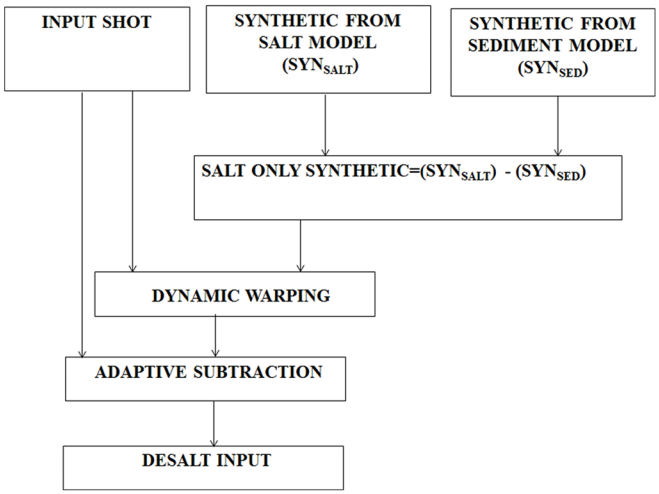

Figure 3. Desalt workflow.

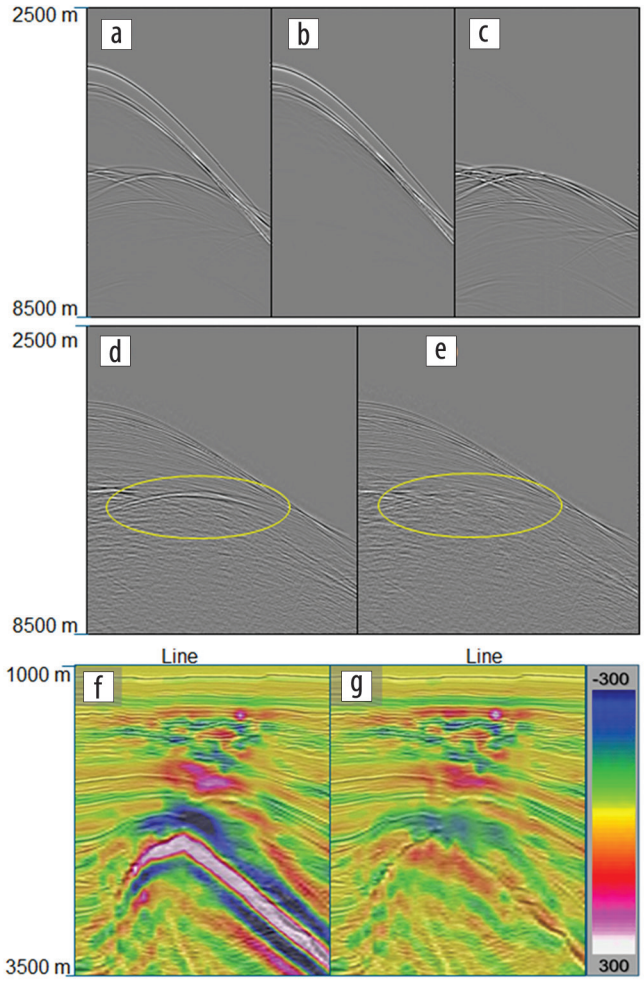

Figure 4. (a) Synthetic from salt including the sediment velocity model. (b) Synthetic from the sediment-only model. (c) Synthetic from the salt-only model. (d) Input shot. (e) Input shot after desalt. (f) FWI ΔV update using input without desalt. (g) FWI ΔV using desalt input.

FWI model update

We begin with the anisotropic velocity model. Throughout FWI, we kept anisotropic parameters (ε and δ) fixed, updating only the velocity. Density is calculated from the velocity using Gardner's relationship (Gardner et al., 1974). An anisotropic wave equation with free-surface boundary condition is used in FWI. A ray-tracing profile is analyzed to identify the maximum depth and offset range for DFWI. Based on the maximum penetration depth from ray tracing, we interpret key horizons on a migrated stack, which are then converted to time and updated to the desalt input shot gather as a mute function during FWI. The mute is applied to the shot gather to keep only the early arrivals for DFWI. Three frequency bands starting from 3 to 12 Hz are selected for FWI. A total of five iterations for each frequency band is applied to update velocity from DFWI. Conventional smoothing approaches during inversion, such as Gaussian filters, do not necessarily preserve the resolution of the model, especially if the smoothing length is larger than the anomaly aiming to be resolved. Smearing of model features across events occurs more frequently under steeply dipping geologic structures. An image-guided smoothing (Hilburn et al., 2014) approach, which automatically detects event continuity and fault features present in the seismic image, is applied to ensure that solutions follow the underlying geology. Image-guided smoothing is applied to the gradient to minimize the footprint and swing noise but at the same time retain the high-frequency details derived by FWI. The DFWI updated model is used as a starting model for RFWI. Diving wave energy from the input data is muted and used as input for RFWI. RFWI is also applied to three frequency bands with five iterations for each frequency band. We update density after each iteration of FWI to minimize the density leakage to the RFWI velocity model updates.

FWI results

Figure 5 shows the refraction and reflection combined FWI results. Figures 5a and 5b indicate the depth slice before and after FWI updates. The depth slice after FWI shows high-frequency details in the model, which were not there in the initial velocity model. The low-velocity anomaly is now more prominent.

Figure 6 shows the crossline view of the FWI results. Figure 6a is the inline section; the amplitude shadow zone indicates the possibility of low-velocity gas-charged sediment. We anticipate a negative velocity update (ΔV) from FWI surrounding the amplitude shadow zone. Figure 6b shows FWI velocity updates corendered on the seismic to highlight the ΔV relation to the seismic. We can see the negative velocity updates derived from FWI surrounding the amplitude shadow zone. Another point to notice on Figure 6b is that the derived FWI model update trend follows nicely with the underlying seismic

image as we apply the image-guided smoothing on the gradient during FWI. Image-guided smoothing of the gradient field leads to the geologically constrained model updates. Figures 6e and 6f show the KDM stack from the initial velocity model and the FWI velocity model, respectively. The FWI model helps improve the continuity of the image highlighted in the circled area. Figures 6g and 6h are gather comparisons from KDM between the initial velocity model and FWI velocity model. The initial velocity model has already gone through one iteration of high-resolution shallow tomography and two iterations of supra-salt tomography to update the velocity model. We can still see a lack of adequate resolution in the model, which may have caused over and under moveout correction of the KDM gather under the highlighted yellow rectangular box (Figure 6g). The KDM gather using FWI did bring the required resolution in the model to help flatten the KDM gather in the highlighted area (Figure 6h) that resulted in improved continuity of the image (Figure 6f). Figure 7 shows a data example extracted along the crossline direction within the surveys. A seismic quiet zone can clearly be seen above the highlighted circled area in Figure 7c. FWI model updates did bring the velocity anomaly associated with the shadow zone (Figure 7b). An improved velocity model from FWI helps improve imaging beneath the shadow zone as well as other highlighted areas in Figure 7c. Event continuity on the KDM gather using the FWI model in KDM is improved when compared to the initial model as shown in Figures 7e and 7f.

Conclusions

We have successfully shown the impact of adapting a desalt workflow on FWI results. Desalt helps remove salt-related energy from the input data, which allows us to use the sediment model as a starting model for entire FWI iterations. Removing or attenuating salt-related energy from the input data reduces the big mismatch between observed and synthetic seismic data near the salt boundary that resulted in eliminating the unstable solution near the salt boundary. This desalt workflow is proven to reduce unrealistic high-velocity updates near the salt. Image-guided smoothing during FWI is applied to perform smoothing constrained by the seismic to retain the high-resolution feature updates brought by FWI. DFWI produces low-frequency background velocity updates to the models. Several iterations of RFWI in addition to DFWI allow us to further fine tune the velocity model in terms of capturing some high-resolution velocity anomalies like gas channels. KDM stack and gather have shown improvement when using the final FWI velocity model over the initial velocity model. TLE

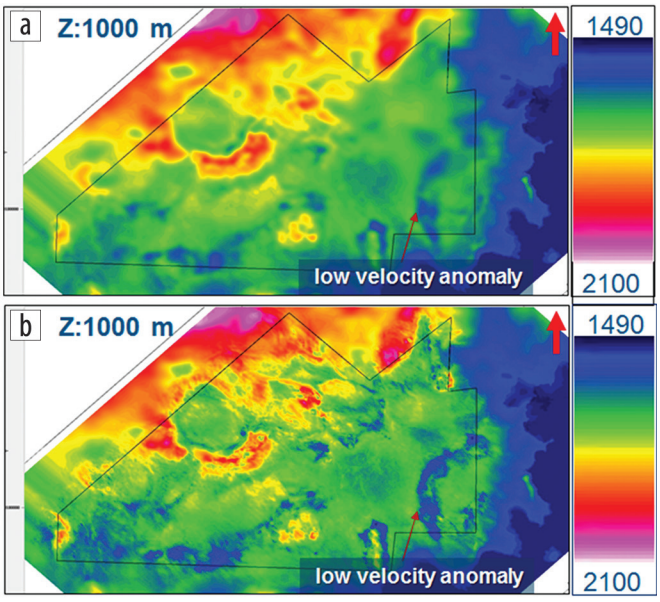

Figure 5. (a) Initial velocity model depth slice. (b) FWI updated velocity depth slice.

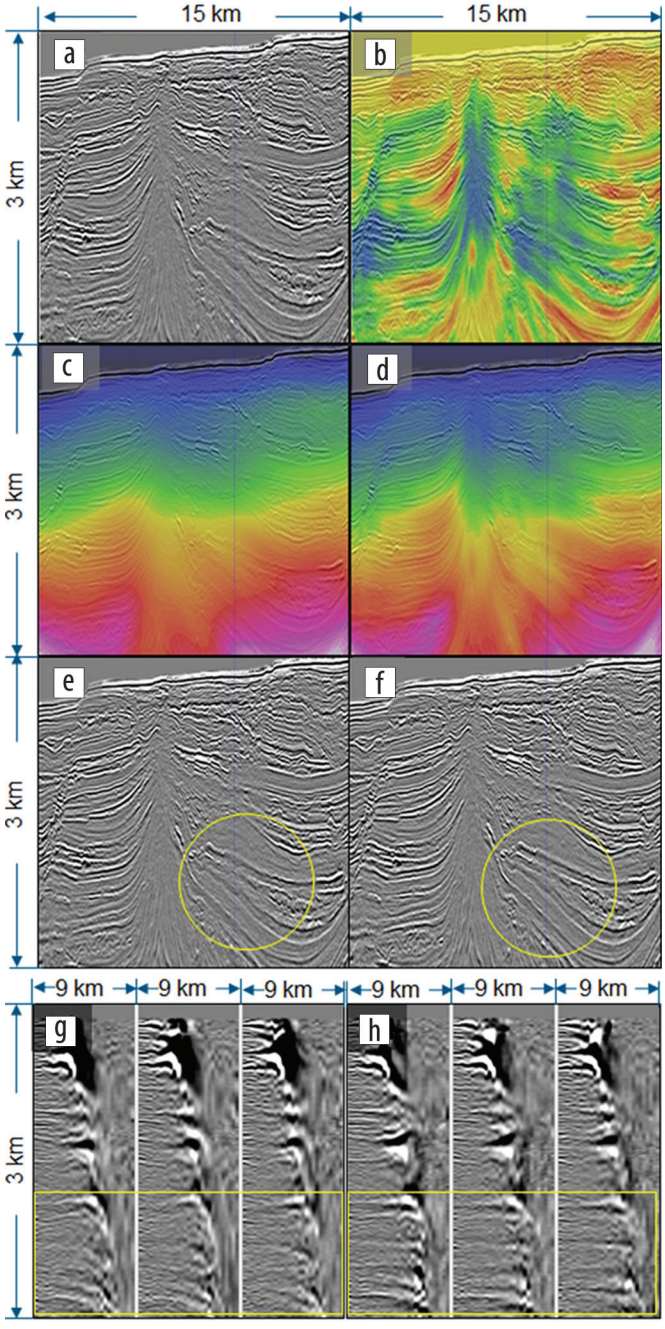

Figure 6. (a) KDM from initial velocity model. (b) FWI velocity updates. (c) Initial velocity model. (d) FWI updated velocity model. (e) KDM stack with initial velocity model. (f) KDM stack from FWI velocity model. (g) KDM gather from initial velocity model. (h) KDM gather from FWI velocity model.

Acknowledgments

The authors would like to thank Zhiming Li and Bin Wang for their contributions. We also thank Connie VanSchuyver for reviewing the manuscript and the management of TGS and WesternGeco Schlumberger for use of the joint-venture data sets in this paper.

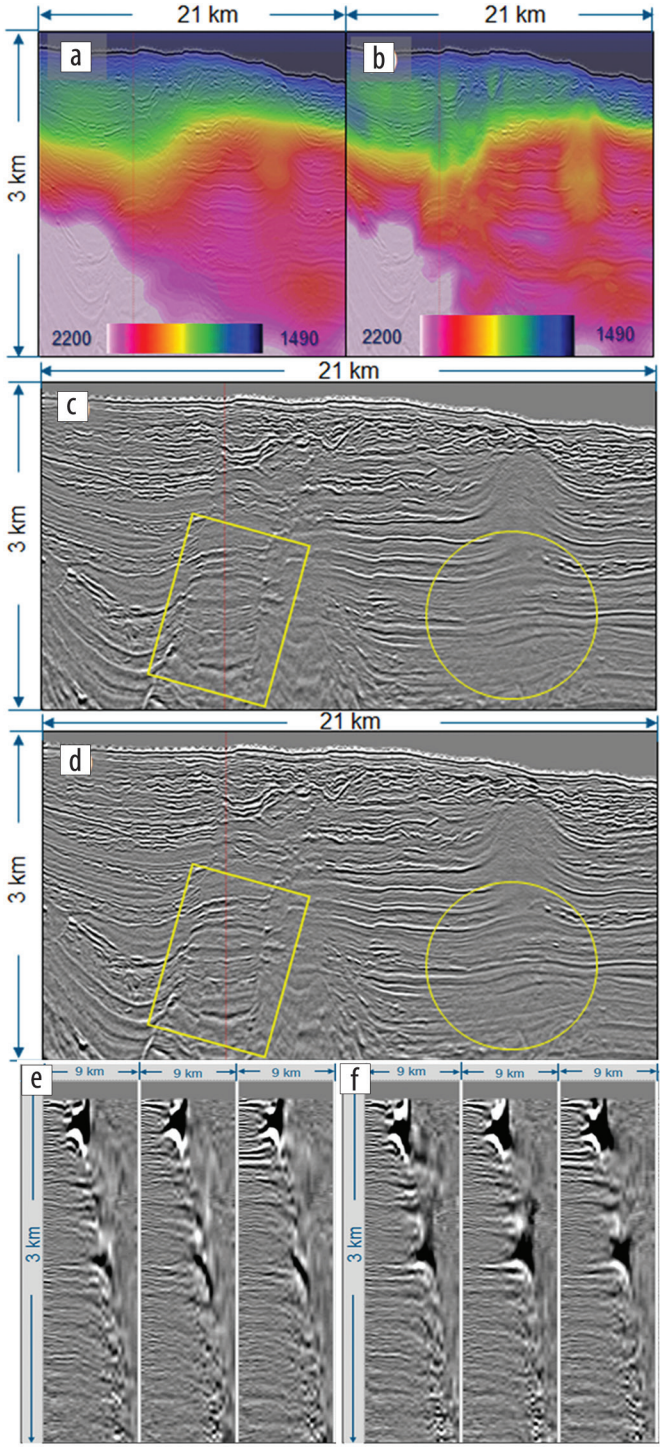

Figure 7. (a) Initial velocity model. (b) FWI updated velocity model. (c) KDM stack with initial velocity model. (d) KDM stack from FWI velocity model. (e) KDM gather from initial velocity model. (f) KDM gather from FWI velocity model.

Data and materials availability

Data associated with this research are confidential and cannot be released.

Corresponding author: dhananjay.tiwari@tgs.com

References

Cai, J., Y. He, Z. Li, B. Wang, and M. Guo, 2009, TTI/VTI anisotropy parameters estimation by focusing analysis, part I: Theory: 79th Annual International Meeting, SEG, Expanded Abstracts, 301–305, https://doi.org/10.1190/1.3255480.

Gardner, G. H. F., L. W. Gardner, and A. R. Gregory, 1974, Formation velocity and density — The diagnostic basics for stratigraphic traps: Geophysics, **39**, no. 6, 770–780, https://doi.org/10.1190/1.1440465.

Jones, I. F., and I. Davison, 2014, Seismic imaging in and around salt bodies: Interpretation, **2**, no. 4, SL1–SL20, https://doi.org/10.1190/INT-2014-0033.1.

Lailly, P., 1983, The seismic inverse problem as a sequence of before stack migrations: Conference on Inverse Scattering, Theory and Application, Society of Industrial and Applied Mathematics, Extended Abstracts, 206–220.

Ma, Y., and D. Hale, 2013, Wave-equation reflection traveltime inversion with dynamic warping and full-waveform inversion: Geophysics, **78**, no. 6, R223–R233, https://doi.org/10.1190/geo2013-0004.1.

Mao, J., J. Sheng, M. Hart, and T. Kim, 2016, High-resolution model building with multistage full-waveform inversion for narrow-azimuth acquisition data: The Leading Edge, **35**, no. 12, 1031–1036, https://doi.org/10.1190/tle35121031.1.

Tarantola, A., 1984, Inversion of seismic reflection data in the acoustic approximation: Geophysics, **49**, no. 8, 1259–1266, https://doi.org/10.1190/1.1441754.

Wang, K., B. Deng, Z. Zhang, L. Hu, and Y. Huang, 2015, Top of salt impact on full waveform inversion sediment velocity update: 85th Annual International Meeting, SEG, Expanded Abstracts, 1064–1069, https://doi.org/10.1190/segam2015-5878985.1.